COOLING OF THE FIBRES IN MINERAL WOOL PRODUCED BY A DOUBLE-DISC SPINNING MACHINE

BOGDAN BLAGOJEVIČ, BRANE ŠIROK*, MARKO HOČEVAR*

School of technologies and systems (VITES),
Na Loko 2, p.p. 111, SI-8000 Novo Mesto, Slovenia
**University of Ljubljana, Faculty of mechanical engineering,*
Aškerčeva 6, SI-1000 Ljubljana, Slovenia

E-mail: bogdan.blagojevic@guest.arnes.si

Submitted May 7, 2008; accepted September 30, 2008

Keywords: Fiber of mineral wool, Cooling, Numerical model, IR-camera

The quality of mineral wool products is affected by the magnitude of fibre thickness. For this reason the paper presents a mathematical model of the cooling of the mineral wool fibres of different thickness on the envelope trajectory of two phase fibre and air flow. On the basis of the results which were obtained by numerical simulations we compared the numerical and experimental results. Experimental results were obtained by using the infra red camera. The results show good agreement between measured surface average fibre temperature in the two phase jet and the numerical results. The numerical model considers also the temperature dependence of thermo-physical properties of the air and mineral wool fibres.

INTRODUCTION

Mineral wool is a general name for many inorganic insulation materials made of fibres. Mineral wool is usually divided into different subgroups depending on the raw materials it is made of, such as rock wool, glass wool and slag wool. The most frequently used raw materials for mineral wool production are diabase, amphibolites, dolomite, granite, basalt, limestone. Because of its amorphous structure, mineral wool has excellent sound and thermal insulation properties. There are several production methods for mineral-wool fibres, with a wide variation of quality and quantity of the final product [1]. The most commonly used mineral wool production process is the 'fiberisation process' of molten rock on fast rotating spinning discs [2-4]. The process of fiberisation includes the transformation of the melt in to the solid structure of fibre form, where the fibre length is significantly bigger than fibre thickness. Molten rock enters the process through a siphon neck into a homogenisation reservoir from where it runs over a 'step' into a channel and then falls under gravity onto the rotating disc of the spinning machine. Fibres are formed from the molten film on the rotating discs. The formation mechanism is described by Eisenklam in [5]. Air is blown coaxially around the discs to transport the fibres away from the spinning machine and into a wool chamber where they solidify into fibres of diameters about 5 μm and lengths greater than 10 mm. The fibre-air flow is schematically shown in the Figure 1. The formation and motion of the fibres depends on the inertial, viscous and surface tension forces within the molten rock film. The breaking mechanism and the formation of the mineral fibres from a spinning machine is briefly described in [4]. The temperature, position and internal tension of each fibre are calculated during the formation phase according to the effects of the inertial and aerodynamic forces. The material that has not been transformed into fibres remains in the form of solidified shots resulting from an incomplete fiberisation process [2, 3, 6]. The quality of the final product depends on the structure of fibres and on the proportion of solidified shots in the mineral wool. Multiple regression model of the mineral fibre thickness are presented in the [6, 7].

This paper presents the influence of the initial and boundary conditions on the cooling of the mineral wool fibres in the fiberisation process of molten rock.

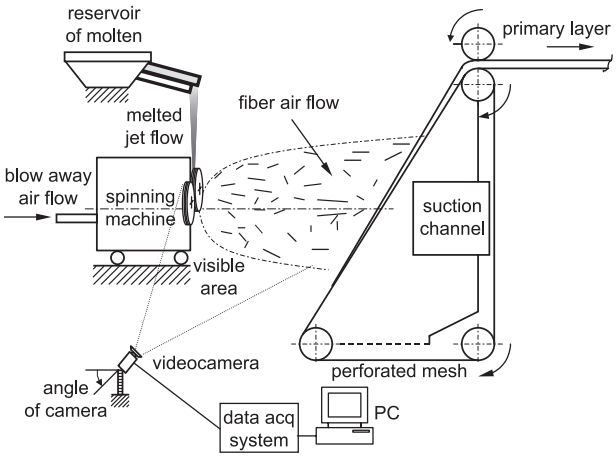

Figure 1. The fibre production process.

For this reason we introduced the mathematical model which enabled computer simulation of the cooling of mineral wool fibres. The temperature drop in the cooling of mineral wool fibres was evaluated experimentally by using the IR-camera. Experiments enabled the estimation of average temperatures on the surface of the fibres - air flow. This will allow the comparison between the measured temperature and the calculated temperature of the fibre.

THEORETICAL

Heat transfer equation

For a better understanding of the fiberisation process, it is also appropriate to present the dynamic and thermodynamic laws of heat transfer in the process of fibre formation [8, 9]. Let us suppose that a fibre with mass m, volume V, surface A, specific heat at a constant pressure c_p and temperature T is moving with velocity $\vec{w}$. If this fibre enters the air flow which has the velocity $\vec{U}$ and temperature T_a, boundary layer is formed around the surface of the fibre, within which the joint resistance against heat transfer ($T \neq T_a$) is combined. Because of the relative movement of the fibre according to the surrounding air flow, only convective heat transfer prevails.

$$\frac{\partial}{\partial t}(m \cdot cp \cdot T) = -\alpha \cdot A \cdot (T - T_a), \qquad (1)$$

where α is the convective heat transfer coefficient. In the spinning melt of inorganic glasses, where temperatures reach 1100-1500°C, the contribution of radiative heat transfer is considerable. The apparent heat transfer for radiation Q_r is equal

$$Q_r = \varepsilon \cdot \sigma \cdot A \cdot ((T + 273.15)^4 - (T_{\text{amb}} + 273.15)^4), \qquad (2)$$

where ε is emissivity, σ is Stefan-Boltzmann constant, T_{amb} is the ambient surface temperature and T is the fiber temperature in °C. If the material and thermodynamic characteristics of the mineral wool fibre are constant, and if we consider radiation, than Equation (1) is transformed into an ordinary differential equation with constant coefficients:

$$\frac{dT}{dt} + \frac{\alpha \cdot A}{m \cdot cp} \cdot (T - T_a) + \frac{\varepsilon \cdot \sigma \cdot A}{m \cdot cp} \cdot \left[(T + 273.15)^4 - (T_{\text{amb}} + 273.15)^4 \right] = 0. \qquad (3)$$

Convective heat transfer coefficient α can be expressed with the aid of Nusselt number Nu, which is dependent on the heat conductivity of air λ_a and the characteristic length (cylinder diameter) of the fibre d:

$$Nu = \frac{\alpha \cdot d}{\lambda_a}. \qquad (4)$$

The differential equation of convective fibre cooling can be written as follows:

$$\frac{dT}{dt} + \frac{Nu \cdot \lambda_a \cdot A}{m \cdot cp \cdot d} \cdot (T - T_a) + \frac{\varepsilon \cdot \sigma \cdot A}{m \cdot cp} \cdot \left[(T + 273.15)^4 - (T_{\text{amb}} + 273.15)^4 \right] = 0. \qquad (5)$$

If we suppose that the cylinder-shaped fibres have diameter d, length l_f and density ρ, Equation (5) can be simplified as follows:

$$\frac{dT}{dt} + 4\frac{Nu \cdot \lambda_a}{\rho \cdot d^2 \cdot cp} \cdot (T - T_a) + 4\frac{\varepsilon \cdot \sigma}{\rho \cdot cp \cdot d} \cdot \left[(T + 273.15)^4 - (T_{\text{amb}} + 273.15)^4 \right] = 0. \qquad (6)$$

In order to solve the Equation (6), we have to know the velocity field around the fibre. The calculation of heat transfer coefficient is in the case of convective transfer mostly dependent on velocity conditions. For laminar flow around the cylinder-shaped fibre, Nusselt number can be calculated on the basis of the following empirical correlation [4, 9]:

$$Nu = 0.4 Re_r^{0.3}, \qquad (7)$$

where Reynold's number can be defined according to the radius of the cylinder-shaped fibre:

$$Re_r = \frac{\left|\vec{w} - \vec{U}\right| \cdot r}{\nu_a}, \qquad (8)$$

where ν_a is the kinematic viscosity of air. Equation (7) is valid for $Re_r < 10^2$ and $Re_l > 10^5$ where Reynold's number Re_l refers to the length of the fibre l [9].

There are other several expressions for the calculation of heat transfer coefficient. Ziabacki [9] gave several expressions on the basis of which we can conclude that $Nu = Nu(Re)$. Hoikka and Westerlund [4] have with experimental work developed the following expression for calculation of Nusselt number:

$$Nu = 0.226 Re_d^{0.611} + 0.469. \qquad (9)$$

Since these authors could not simulate the velocity of up to 100 m/s, they had to extrapolate the equation. Lindquist's equation is also very similar:

$$Nu = 0.48 Re_d^{0.5} + 0.43. \qquad (10)$$

Next, we present Sano's model [10]:

$$Nu = 0.15 Re_d^{0.36} + 0.25. \qquad (11)$$

In our model we are used the Equation (9).

Trajectories of the mineral wool fibres

In the process of mineral wool production, the melt jet is flowing onto the centrifuge. Small fibres are formed out of the thin melt film on the rotating wheels. Thin

fibres intertwine in the turbulent airflow and go over from radial into axial direction of the carrying coaxial airflow. This airflow usually surrounds the circumference of the rotating wheels. At the nozzle outlet, it reaches high velocities (higher than 100 m/s). In this section we will describe the kinematics of the two-phase jet of mineral wool fibres and axial air flow. Our model is based on the following assumptions:

- the jet flow of fibres and the air flow are stationary and one-dimensional;
- when determining the flow, we observe only the fibre trajectories which define the outer envelope of the jet y_e and tangentially leave the rotating wheel as shown in Figure 2;
- the radius of flow of fibres curvature changes along the x axis;
- air enters into the jet with constant velocity rectangular to the jet envelope [11, 12];
- temperature of the air T_a is constant;
- fibres are cylinder-shaped and have diameter d , length l_f, and temperature T;
- the initial fiber temperature is constant and equal T_f;
- density of the melt is calculated according to the [7, 13, 14, 15];
- thermo-physical properties for humid air are taken from [16].

Fibre trajectory on the jet envelope

The jet envelope is determined by the outer trajectories of the fibres. The movement of fibres along the envelope is mostly influenced by the drag force $\vec{F}_u$, which is a result of relative movement between the fibres and air [4, 11, 12]:

$$\overrightarrow{F_u} = -\frac{1}{2}\cdot c_f \cdot A_k \cdot \rho_a \cdot \left|\overrightarrow{w_{fe}} - \overrightarrow{U_e}\right| \cdot \left(\overrightarrow{w_{fe}} - \overrightarrow{U_e}\right), \qquad (12)$$

where c_f is a drag coefficient of a fibre, A_k is the front surface of a fibre, ρ_a is air density, $\vec{w}_{fe}$ is fibre velocity on the jet envelope and $\vec{U}_e$ is the velocity of the air flow entering rectangular to the envelope. Besides the resisting force that drags the fibre movement, we also consider the gravity force of the fibre $\vec{F}_g$ and the buoyancy force $\vec{F}_b$ [4, 11, 12].

$$\overrightarrow{F_g} + \overrightarrow{F_b} = \left(\rho_f - \rho_a\right)\cdot V_f \cdot \vec{g}, \qquad (13)$$

where ρ_f is fibre density, V_f is fibre volume and $\vec{g}$ is acceleration due to the gravity. The momentum equation for fibre movement along the envelope is:

$$\frac{d\left(m\overrightarrow{w_{fe}}\right)}{dt} = \overrightarrow{F_u} + \overrightarrow{F_g} + \overrightarrow{F_b}\ . \qquad (14)$$

If we consider that fibres, moving along the envelope, are cylinder-shaped and have diameter d and length l_f, the Equation (14) can be expressed as [4, 11, 12]:

$$\frac{d\left(m\overrightarrow{w_{fe}}\right)}{dt} = -\frac{1}{2}\cdot c_f \cdot A_k \cdot \rho_a \cdot \left|\overrightarrow{w_{fe}} - \overrightarrow{U_e}\right| \cdot$$

$$\cdot\left(\overrightarrow{w_{fe}} - \overrightarrow{U_e}\right) + \left(\rho_f - \rho_a\right)\cdot V_f \cdot \vec{g}. \qquad (15)$$

Supposing the air enters rectangular to the jet envelope [11, 12], (see Figure 2), the absolute value of relative velocity vector $\vec{w}_{fer}$ is:

$$\left|\overrightarrow{w_{fer}}\right| = \left|\overrightarrow{w_{fe}} - \overrightarrow{U_e}\right| = \sqrt{w_{fe}^2 + U_e^2}\,. \qquad (16)$$

By considering the stationary flow and the projections of momentum Equation (15) onto the tangent of jet envelope, we get:

$$\frac{dw_{fe}}{dx} = -\frac{1}{2}\cdot c_{ft}\cdot\frac{1}{l_f}\cdot\frac{\rho_a}{\rho_f}\cdot\sqrt{w_{fe}^2 + U_e^2} \mp$$

$$\mp\frac{\left(\rho_f - \rho_a\right)}{\rho_f}\cdot g\cdot\frac{\cos(\beta)}{w_{fe}}\ , \qquad (17)$$

where the upper or the lower envelope determines the sign $\mp$. The curvature radius of jet envelope R is defined as follows [11]:

$$\frac{1}{|R|} = \frac{a_n}{w_{fe}^2} = \frac{|y_e''|}{\sqrt{\left(1 + y_e'^2\right)^3}}\ , \qquad (18)$$

where a_n is a normal acceleration component of the fibre, y_e' and y_e'' are the first and the second derivation of the envelope on axis x. When considering the stationary melt flow, the resultant of all forces exerting on the envelope is rectangular to the direction of the tangent:

$$\rho_f \cdot V_f \cdot a_n = F_{un} + \left(F_g - F_b\right)\cdot\sin(\beta)\ , \qquad (19)$$

where the following was taken into consideration

$$\sin(\beta) = \frac{dx}{\sqrt{(dx)^2 + (dy_e)^2}}\ . \qquad (20)$$

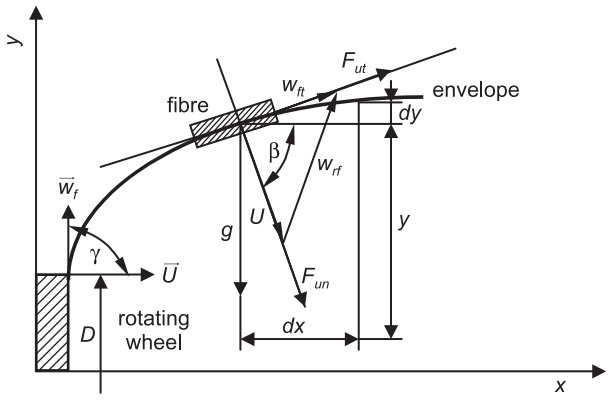

Figure 2. Fibre trajectory on the jet envelope.

F_{un} is the component of the drag force rectangular to the direction of the tangent. If we consider the curvature sign, the second derivation can be expressed as $y''_e = d^2y_e/dx^2$

$$y''_e = \frac{d^2 y_e}{dx^2} = -\frac{1}{2}\cdot c_{fn}\cdot\frac{1}{l_f}\cdot\frac{\rho_a}{\rho_f}\cdot\sqrt{w_{fe}^2+U_e^2}\cdot \cdot\frac{U_e}{\sin^3(\beta)}\cdot\frac{1}{w_{fe}^2}\mp\frac{(\rho_f-\rho_a)}{\rho_f}\cdot g\cdot\frac{1}{\sin^2(\beta)}\cdot\frac{1}{w_{fe}^2} \quad , \tag{21}$$

where the upper or the lower envelope determines the sign $\mp$. The resistance coefficient of the fibre in the air flow depends mostly on the Reynold's number. In order to calculate the resistance coefficient in direction of the tangent, Glicksman in [8] offers the following expression:

$$c_{ft} = 0.4\cdot Re_r^{-0.7},\ Re<100, \tag{22}$$

where Reynold's number refers to the radius of cylinder-shaped fibre:

$$Re_r = \frac{|w_{ret}|\cdot d}{2\cdot\nu}, \tag{23}$$

where $|w_{ret}|$ is relative velocity of fibre in the tangentially directed air flow, d is fibre diameter used for calculating the drag coefficient c_{ft}, v is the kinematic viscosity of air. Drag coefficient of the fibre c_{fn} in rectangular direction can be calculated from the following empirical expression [9]:

$$c_{fn} = 1.018+1.458\cdot Re^{-0.5}+8.151\cdot Re^{-0.8},\ Re>0.06, \tag{24}$$

where Reynold's number is defined as:

$$Re = \frac{|w_{ren}|\cdot d}{\nu}, \tag{25}$$

where $|w_{ren}|$ is relative velocity of fibre in the normally directed air flow.

EXPERIMENTAL

Thermovision of the fibre-air flow

The temperature measurements of the fibre-air flow have been performed using the thermal vision method [17, 18]. The experiments were performed on a double-disc spinning machine in a real production process, (Figure 1). The diameter of both cylindrically shaped 120 mm wide discs, was 385 mm. The temperature distribution on the first and second rotating disc has been assumed to be equal and axi-symmetrical, because of experimental limitations.

Measurements of the fibre-air temperature were performed using a fast infrared (IR) sensitive camera Thermosensorik CMT384SM. The camera uses a cooled mercury cadmium telluride Focal Plane Array (FPA) detector, which consists of a matrix with 384×288 elements/pixels. It is optimized for the range of wavelengths between 3 μm and 5 μm. Its thermal sensitivity is < 0,15 K. The camera should be calibrated prior to the measurements. The measurement uncertainty is depended on the type and quality of the calibration method.

The IR camera was placed at the angle of 52° to the second wheel's longitudinal axis of the spinning machine. The distance between the IR camera and the discs was 3,6 m. A high temperature filter was used during experiments. The position of the IR camera is shown schematically in Figure 1. 1000 images were recorded in series and stored to disk. The exposure time was 0.05 ms. Sample image is shown in Figure 3.

The uncertainty of the measurements of the fibres temperature is seriously limited due to the very small quantity of fibres in selected volume under observation. Fibres are distributed mainly along the fibre trajectory, and the camera measures the background temperature when fibres are not present in high enough density. We have thus included in analysis only five percent of measurement data with the highest temperature on each location on the fibre trajectory. Other values were rejected because we have assumed that the background was visible through the fibres and hence the measured temperature was too low. The analysis was performed using Matlab software.

The thermal vision camera was calibrated prior to the measurements using the hot cilinder plate with diameter 150 mm and thickness 40 mm with installed thermocouple sensor. According to the calibration procedure calibration was performed at two temperatures.

COMPARISON OF NUMERICAL AND EXPERIMENTAL RESULTS

When determining the fibre trajectories along the envelope, the following supposition was taken into consideration:

$$\frac{dw_{fe}}{dt} = w_{fe}\frac{dw_{fe}}{dx}\ . \tag{26}$$

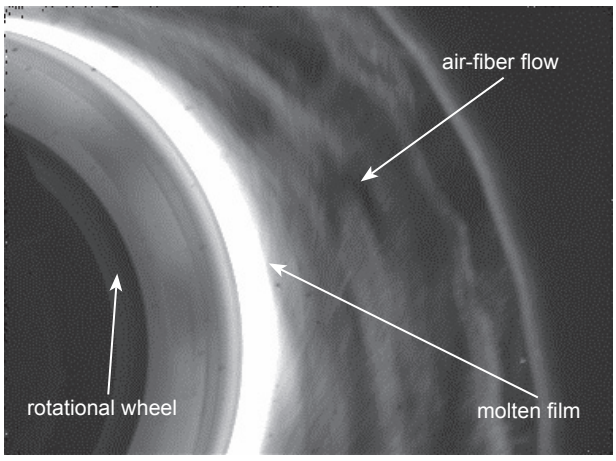

Figure 3. Sample thermal vision image.

A similar supposition can be used when observing the fibre cooling:

$$\frac{dT}{dt} = w_{fe}\frac{dT}{dx} \ . \tag{27}$$

With regard to Equation (26), Equation (5) can again be expressed as:

$$\frac{dT}{dx} = -4\frac{\alpha}{\rho_f \cdot w_{fer} \cdot d_f \cdot cp_f}\cdot(T - T_a) - 4\frac{\varepsilon\cdot\sigma}{\rho\cdot cp\cdot d\cdot w_{fer}}\cdot$$

$$\cdot\left[(T+273.15)^4 - (T_{\text{amb}}+273.15)^4\right] \tag{28}$$

If we want to describe the fibre trajectory on the jet envelope and the fibre cooling, we have to simultaneously solve the following system of Equations (17), (21) and (28). This system of equations can be solved with the Runge-Kutta method of 4th order. Optimal step is determined according to the initial and boundary conditions. For calculation we used the following settings: average fibre thickness is 5 μm and three different length of the fibres 1 mm, 10 mm and 100 mm. The initial temperature of fibres is 1450°C, average air temperature is 30°C. Fibres are formed at the circumference of the wheel and start to move in direction of *y* axis, the air flow is moving in direction of *x* axis rectangular to the fibre with velocity of 100 m/s. The emissivity was equal 0.85. The optimal step (0.1 μm) for solving the system of equations was chosen according to the initial and boundary conditions. Numerical results of the fibre trajectory and fibre temperatures along the trajectory on the jet envelope are shown in Figures 4 and 5.

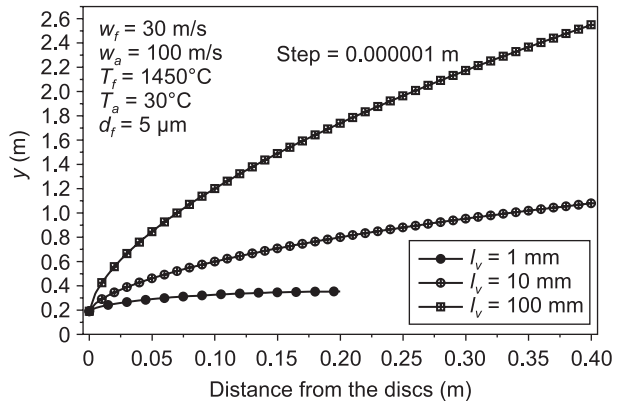

Figure 4. Fibre trajectory on the jet envelope.

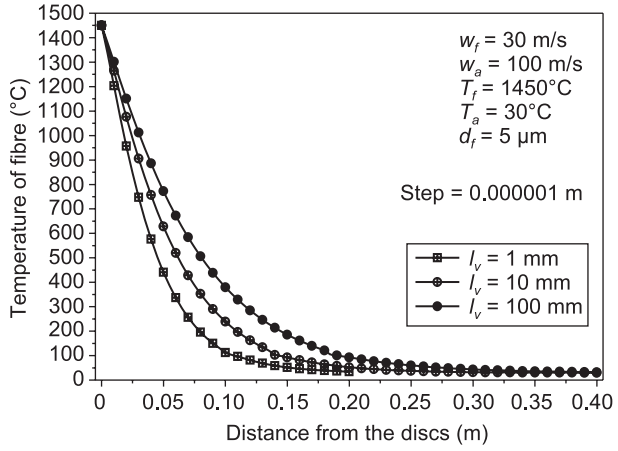

Figure 5. Fibre temperature along the trajectory on the jet envelope.

On the way along the jet envelope, the fibre was constantly cooling. The Figure 5 shows the temperature of the fibre on its way along the jet envelope.

If we substitute size distribution of the mineral wool fibers with the average diameter *d* and length l_f, the obtained numerical results which are shown in the Figure 5 can be directly used. The numerical simulations are made for different lengths and diameters of the fibers, the others input quantity are the same as in the numerical simulations which are present in the Figures 4 and 5. If the position of the IR-camera is considered, we can transform the experimental results on the envelope of the two phase jet. The transformed results are shown in the Figure 6, which presents dependence between non-dimensional temperature

$$\theta = \frac{T - T_a}{T_f - T_a}\ , \tag{29}$$

and the distance from the discs, where T_f is the initial fibre temperature.

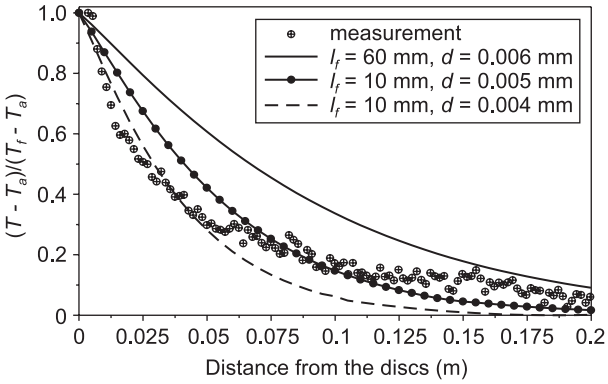

Figure 6. Comparison between experimental and numerical prediction results of the temperature in the two phase fiber and air flow.

CONCLUSIONS

The presented numerical algorithm enables the prediction of the cooling process of fibres. The model enables various input parameters such as fibre diameter, fibre length, initial temperature of the air and fibres and initial velocity. Numerical values are in good agreement with the experimental procedure based on using the IR-camera. The discrepancies between the numerical

values and experimental values can be results of the non-knowing the initial velocity field around the fibres. The diagrams of the cooling fibres are very dependent on the length of the fibres. On the basis of such diagrams we can evaluate the cooling process of a fibre. The experimental IR-procedure can be used in the real production of mineral wool fibres.

References

1. Ohberg I.: Ann. Occup. Hyg. *31*, 529 (1987).
2. Trdič F., Širok B., Bullen P., Philpott D. R.: Real Time Imaging *5*, 125 (1999).
3. Angwafo A. W., Bullen P., Philpott D. R.: Proceeding of the FEDSM'98. ASME Fluids Engineering Division Summer Meeting, 21-25 June, Washington 1998.
4. Westerlund T., Hoikka T.: Computers Chem. Engng. *13*, 1153 (1989).
5. Eisenklam P.: Chem. Eng. Sci. *19*, 693 (1963).
6. Blagojević B., Širok B.: Glass Technol. *43*, 120 (2002).
7. Blagojević B., Širok B., Štremfelj B.: Ceramics-Silikáty *48*, 128 (2004).
8. Glicksmann L. R.: Glass Technol. *9*, 131 (1968).
9. Ziabacki A.: *Fundamentals of fibre formation*, Wiley, New York 1976.
10. Sano Y.: *Formation of Fibres and Development of Their Structure*, Edited by The Society of Fiber Science and Technology, Japan 1969.
11. Rothe P. H., Block J. A.: Int. J. Multiphase Flow *3*, 263 (1976).
12. St-Georges M., Buchlin J. M.: Int. J. Multiphase Flow *20*, 979 (1994).
13. Lange R. A., Carmichael I. S. E.: Geochimica et Cosmochimica Acta *51*, 2931 (1987).
14. Courtial P., Dingwell D. P.: American Mineralogist *84*, 4645 (1999).
15. Lakatos T., Johannson L. G., Simmingsköld B.: Glasteknisk Tidskrift *36*, 51 (1981).
16. Blagojević B., Bajsić I.: Heat mass transf. *31*, 435 (1996).
17. Stanjko D., Lakota M., Hočevar M.: Comput. Electron. Agric. *42*, 31 (2004).
18. Širok B., Blagojevič B., Bullen P. Glass Technol. *46*, 334 (2005).

Symbols

A	Surface of a fibre, (m^2)
A_k	Front surface of a fibre, (m^2)
a_n	Normal acceleration, (m/s^2)
c_f	Drag coefficient, (/)
c_{ft}	Drag coefficient of the fibre in direction of the tangent, (/)
c_{fn}	Drag coefficient of the fibre in rectangular direction, (/)
cp	Specific heat at constant pressure, (J/kgK)
d	Diameter of the fibre, (m)
D	Diameter of the rotating wheel, (m)
F_b	Buoyancy force, (N)
F_g	Gravity force, (N)
F_u	Drag force, (N)
F_{un}	Drag force rectangular to the direction of the tangent, (N)
F_{ut}	Drag force in the direction of the tangent, (N)
g	Gravitational acceleration, (m/s2)
l_f	Length of the fiber, (m)
m	Mass of the fiber, (kg)
Nu	Nusselt number, (/)
Q_r	Radiation heat flux, (W)
r	Radius of the fibre, (m)
R	Radius curvature of the jet envelope, (m)
R_e	Reynolds number, (/)
t	Time, (s)
T	Temperature, (K)
T_a	Air temperature, (K)
T_{amb}	Ambient temperature, (K)
T_f	Initial temperature of the fiber, (K)
U	Velocity vector of the air, (m/s)
U_e	Air velocity on the envelope, (m/s)
V_f	Fibre volume, (m3)
w_f	Velocity vector of the fiber, (m/s)
w_{fe}	Fiber velocity on the envelope, (m/s)
w_{fer}	Relative velocity vector, (m/s)
$\lvert w_{ret}\rvert$	Relative velocity of fibre in the tangentially direction, (m/s)
x, y	Cartesian coordinates, (m)
y_e	direction of envelope, (m)
y_e'	First derivation of the envelope on axis x, (m/m)
y_e''	Second derivation of the envelope on axis x, (m/m^2)

Greek symbols

α	Convective heat transfer coefficient, (W/m^2K)
β	Angle, (°)
γ	Initial angle between velocity vectors of the air and fiber, (°)
ε	Emissivity, (/)
λ_a	Conductive heat coefficient of the air, (W/mK)
ν_a	Kinematic viscosity of the air, (m^2/s)
ρ_f	Density of the fibre, (kg/m^3)
ρ_a	Density of the air, (kg/m^3)
σ	Stefan-Boltzmann constant, (W/m^2K^4)